

Received June 24, 2020, accepted July 7, 2020, date of publication July 10, 2020, date of current version July 23, 2020.

Digital Object Identifier 10.1109/ACCESS.2020.3008608

A Study of the COVID-19 Impacts on the Canadian Population

JOHN YAWNEY¹ AND STEPHEN ANDREW GADSDEN², (Senior Member, IEEE)

¹Department of Data Science and Artificial Intelligence, Adastral Corporation, Markham, ON L3T 7M8, Canada

²College of Engineering and Physical Sciences, University of Guelph, Guelph, ON N1G 2W1, Canada

Corresponding author: John Yawney (john.yawney@adastragr.com)

ABSTRACT With the recent outbreak of COVID-19, the reach and scale of COVID-19 cases is top of mind for everyone and many research groups are actively monitoring and exploring the potential spread. A positive consequence of past epidemics and pandemics is that there are sound epidemiological compartmental modelling approaches that can effectively model disease spread. With minor changes to the underlying dynamical system of equations, many different strategies and situations can be explored. In particular, one such strategy of social distancing is top of mind for many Canadians as our political leaders, local businesses, and fellow Canadians promote and adopt this approach with the hopes that it will effectively ‘flatten the curve’ and reduce or prevent further spread. In this paper, the baseline *SIR* model is introduced with its close counterpart, the *SEIR* model. Social distancing is modelled through the isolation of a subset of the susceptible population and comparative studies are performed considering a range in the proportion of individuals isolated. Robust and accurate numerical approximation techniques are used to simulate the pessimistic base case for which no preventative measures are taken and for various social distancing regimes. The results of social distancing are consolidated into two groups – those that flatten the curve and those that completely halt the disease spread. Mathematical formulations show that the turning point between these two regimes is when the effective reproductive rate, denoted R_e , is equal to 1. Conclusions are made regarding the impacts and extent of the spread in relation to the severity of social distancing measures.

INDEX TERMS COVID-19, epidemiology, infectious disease modeling, social distancing.

I. INTRODUCTION

As the COVID-19 outbreak continues and expands rapidly into numerous countries, governmental bodies are starting to move toward conventional containment and response tactics, such as isolation and social distancing. It has been observed that these have a dramatic impact on the flattening of the curve and reduction of the virus spread [1]. There have been observational studies that have demonstrated how these strategies reduce the virus caseloads [2]–[5] as well as simulations performed by COVID-19 response teams showing the progression under different paradigms.

Several articles focused on the COVID-19 pandemic have recently been published in the literature. Authors have studied the effects of social media and its use to acquire and exchange situational information so that relevant and accurate information is provided to the population [6]. Early prediction of the COVID-19 outbreak in mainland China has also been considered using simple mathematical models and limited

data released to the public [7]. The authors discovered that a part of the released data was unreasonable and had to be discarded. This highlights the importance of utilizing reliable sources of data to develop accurate infectious disease models that health officials can use to educate and inform politicians on best practices for the public.

In an attempt to slow the spread of COVID-19, the Canadian government, working with provincial and territorial counterparts, enacted a number of measures. These measures include social distancing efforts, limiting the size of public gatherings, closing schools and other public buildings, shuttering of malls and non-essential commercial districts, and restricting non-essential travel in and out of Canada. In an effort to mitigate the economic impacts, the Canadian government provided funding for individuals and families through the Canada Emergency Response Benefits (CERB) and the Canada Child Benefit (CCB) programs. Furthermore, wage subsidies were introduced to avoid layoffs, rehiring of employees, and help create new jobs. Financial support was also provided to businesses through interest free loans, tax deferral programs, and investments in industry.

The associate editor coordinating the review of this manuscript and approving it for publication was Derek Abbott¹.

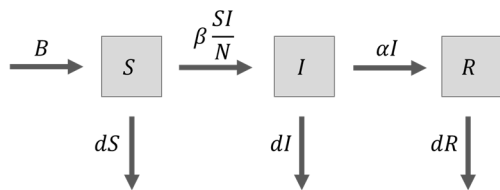


FIGURE 1. Standard SIR model dynamics.

This paper aims to target both a specific population, the Canadian population, and demonstrates the impacts various social distancing and isolation strategies have on either flattening the curve or halting the spread based on the severity of the social distancing measures. The two categories of simulations are partitioned into those with an effective reproductive rate above but nearing 1 and those for which the effective reproductive rate drops below 1. This paper also compares how the various strategies influence the required amount of time to reach a disease-free population state.

The paper is organized as follows. Two types of traditional compartmental models are described in Section II, followed by proposed models used to study COVID-19 impacts introduced in Section III. In Section IV, computer simulations under various pandemic scenarios are described, and the results are presented and discussed. Section V outlines some of the limitations of the current paper with notes on future improvements. Section VI contains further remarks on the findings followed by conclusions outlined in Section VII.

II. COMPARTMENTAL MODELS

Compartmental models are a system of ordinary differential equations used to model the spread of infectious diseases. This section provides an overview of two of the most common compartmental modelling definitions.

A. SIR MODEL

In disease modelling, the simplest compartmental model takes the form of an *SIR* model. If we assume that the disease will cause immediate infection in susceptible individuals, then each susceptible individual instantaneously becomes infectious and then later recovers [8]. This is called an *SIR* model, where *S* represents the susceptible class, *I* the infected class, and *R* the recovered, or removed, class. In this model, α is used to denote the recovery rate, so that $1/\alpha$ is the mean length of the transmission period. The serial interval is simply this mean length of transmission and we obtain the state-space transition diagram outlined in Fig. 1.

Using the notation \dot{X} to denote the time derivative of compartment *X*, the *SIR* mathematical model can be written as the following system of differential equations:

$$\dot{S} = B - dS - \beta \frac{SI}{N} \tag{1}$$

$$\dot{I} = \beta \frac{SI}{N} - dI - \alpha I \tag{2}$$

$$\dot{R} = \alpha I - dR \tag{3}$$

B. SEIR MODEL

Although the *SIR* model does have some interesting properties it is not as realistic as its more advanced counterpart, the *SEIR* model. In this type of compartmental model, a susceptible individual is assumed to come in contact with an infected individual and then moves into a latent exposed (*E*) class before becoming infectious (*I*) [8]. It is initially assumed that every susceptible individual has equal likelihood of contacting an infected individual and contracting the virus.

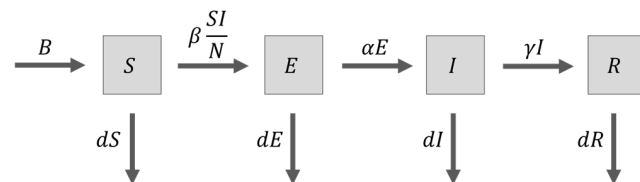


FIGURE 2. Standard SEIR model dynamics.

If *B* is the birth rate and we use the simplification of a constant population size, then $B = dN$, where *d* is the per capita death rate and *N* is the total population size. Assuming the more general four compartment *SEIR* model, $N = S + E + I + R$. β is a transmission rate, the effective contact rate of infected individuals [8], under the well-mixed assumption. We incorporate the law of mass action, which states that the number of new infections depends on the product of the number of infected individuals, the number of susceptible individuals, and a transmission parameter [9]. α is the rate at which we progress from the exposed class to the infectious class, so that $1/\alpha$ is the mean length of the incubation period. γ is the recovery rate, so $1/\gamma$ is used as the mean length of the transmission period. Therefore, the mean generation time or serial interval for the *SEIR* model introduced is $G = 1/\alpha + 1/\gamma$ [10]. In this case, the state-space transition diagram takes the form as shown in Fig. 2.

Including (1), the following system of differential equations represent the *SEIR* model defined in Fig. 2:

$$\dot{E} = \beta \frac{SI}{N} - dE - \alpha E \tag{4}$$

$$\dot{I} = \alpha E - dI - \gamma I \tag{5}$$

$$\dot{R} = \gamma I - dR \tag{6}$$

We note that this model does not incorporate a term for disease-induced deaths.

III. MODELS FOR PREDICTING DISEASE

In this section, the stability analysis and computation of β is considered, followed by the effects of variable birth and death rates, the incorporation of disease-related deaths, and media effects such as social distancing.

A. STABILITY ANALYSIS AND COMPUTATION OF β

Using the Jacobian (first-order Taylor series approximation) and stability conditions for an *SIR* model, the basic

reproductive number R_0 can be found. Considering the disease-free equilibrium $\dot{S} = \dot{I} = \dot{R} = 0$ we get the trivial solution $(S, I, R) = (N, 0, 0)$. Since the recovered class is redundant, we consider the classes S and I and calculate the Jacobian matrix as follows:

$$J(S, I) = \begin{bmatrix} -d - \beta I/N & \beta S/N \\ \beta I/N & \beta S/N - d - \alpha \end{bmatrix} \quad (7)$$

By substituting the disease-free equilibrium, we obtain the following:

$$J(N, 0) = \begin{bmatrix} -d & \beta \\ 0 & \beta - d - \alpha \end{bmatrix} \quad (8)$$

Since $-d$ is always negative, it is required that $\beta - d - \alpha < 0$ for the disease to die out. We know that if $R_0 < 1$, the disease will die out so:

$$\beta - d - \alpha < 0 \Rightarrow \beta < d + \alpha \Rightarrow R_0 = \frac{\beta}{d + \alpha} < 1 \quad (9)$$

However, when analyzing the stability of the *SEIR* model the next-generation method is typically used to effectively calculate the basic reproduction number [11]. In this method, we define the vector $\mathbf{x} = \{x_i : i = 1, \dots, n\}$ as the distribution of the number of individuals in each compartment. We next let $F_i(\mathbf{x})$ be the rate of appearance of new infections in compartment i and $V_i(\mathbf{x}) = V_i^-(\mathbf{x}) - V_i^+(\mathbf{x})$ where V_i^+ and V_i^- are the rates of transfer of individuals into and out of compartment i by all other means.

The next generation operator is FV^{-1} where F and V are the matrices defined as follows:

$$F = \left[\frac{\partial F_i(\mathbf{x})}{\partial x_j} \right]_{\mathbf{x}=\mathbf{x}_0} \quad \text{and} \quad V = \left[\frac{\partial V_i(\mathbf{x})}{\partial x_j} \right]_{\mathbf{x}=\mathbf{x}_0} \quad (10)$$

where $i, j = 1, \dots, m$ and where \mathbf{x}_0 is the disease-free equilibrium. R_0 is given by the spectral radius of the next-generation operator [11].

Considering the standard *SEIR* model proposed above, we consider the compartments E and I since interest is in the spread of the infection. We write these compartments in their simplified forms:

$$\dot{E} = \beta \frac{SI}{N} - (d + \alpha) E \quad (11)$$

$$\dot{I} = \alpha E - (d + \gamma) I \quad (12)$$

The disease-free equilibrium is $\mathbf{x}_0 = (N, 0, 0, 0)$. Then $F_2(\mathbf{x}) = \beta SI/N$ and $F_3(\mathbf{x}) = 0$ so that matrix F can be computed as follows:

$$F = \begin{bmatrix} \frac{\partial F_2(\mathbf{x}_0)}{\partial E} & \frac{\partial F_2(\mathbf{x}_0)}{\partial I} \\ \frac{\partial F_3(\mathbf{x}_0)}{\partial E} & \frac{\partial F_3(\mathbf{x}_0)}{\partial I} \end{bmatrix} = \begin{bmatrix} 0 & \beta \\ 0 & 0 \end{bmatrix} \quad (13)$$

The computations of V_i for $i = 2, 3$ are:

$$V_2(\mathbf{x}) = (d + \alpha) E, \quad V_3(\mathbf{x}) = (d + \gamma) I - \alpha E \quad (14)$$

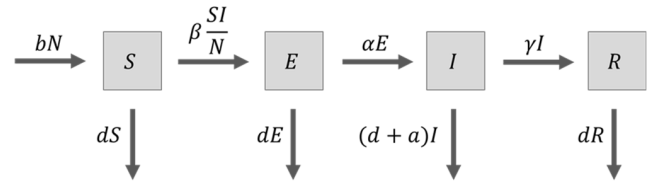


FIGURE 3. SEIR model dynamics with variable birth, death, and disease-related death rates.

The matrix V can now be readily computed as:

$$V = \begin{bmatrix} \frac{\partial V_2(\mathbf{x}_0)}{\partial E} & \frac{\partial V_2(\mathbf{x}_0)}{\partial I} \\ \frac{\partial V_3(\mathbf{x}_0)}{\partial E} & \frac{\partial V_3(\mathbf{x}_0)}{\partial I} \end{bmatrix} = \begin{bmatrix} d + \alpha & 0 \\ -\alpha & d + \gamma \end{bmatrix} \quad (15)$$

Having calculated F and V , the next-generation operator can be calculated as:

$$FV^{-1} = \begin{bmatrix} \frac{\alpha\beta}{(d + \gamma)(d + \alpha)} & \frac{\beta}{d + \gamma} \\ 0 & 0 \end{bmatrix} \quad (16)$$

The spectral radius of this matrix gives the value for the reproductive number R_0 which yields the following relationship:

$$R_0 = \frac{\alpha\beta}{(d + \alpha)(d + \gamma)} \quad (17)$$

The assumption of homogeneity of the population implies that the population can be broken into compartments in which each compartment has identical parameter values for all those individuals in that specific compartment [12]. In more general cases, the basic reproduction number R_0 takes on the definition of “the number of new infections produced by a typical infected individual in a population at a disease-free equilibrium” [13]. Fortunately, for many widespread diseases such as influenza or COVID-19 continuous studies are being performed to estimate R_0 . In this base case, virus spread will be contained when $R_0 < 1$. However, we will see below that with the introduction of strategies such as social distancing that this requirement on R_0 is sufficient but not necessary as disease spread can be halted once the effective reproductive number R_e drops below 1. This value will be defined below in the context of social distancing.

B. VARIABLE BIRTH AND DEATH RATES

In a more realistic scenario, there is varying birth and death rates as well as disease-related deaths. If we denote the birth rate by b , death rate by d , and disease-related death rate by a , then we get the state-space transition diagram outlined in Fig. 3.

In this case, the dynamical system of equations is [14], [15]:

$$\dot{S} = bN - \beta \frac{SI}{N} - dS \quad (18)$$

$$\dot{E} = \beta \frac{SI}{N} - (\alpha + d) E \quad (19)$$

$$\dot{I} = \alpha E - (\gamma + a + d) I \quad (20)$$

$$\dot{R} = \gamma I - dR \tag{21}$$

The total population is also time varying with the following dynamic equation [14], [15]:

$$\dot{N} = \dot{S} + \dot{E} + \dot{I} + \dot{R} = (b-d)N - aI \tag{22}$$

Normalizing by N we have the following:

$$s = \frac{S}{N}, \quad e = \frac{E}{N}, \quad i = \frac{I}{N}, \quad r = \frac{R}{N} \tag{23}$$

Dividing the *SEIR* model defined above by N and subbing for $-d$ within the 4 equations by using the dynamic equation for the total population we get [14]:

$$\dot{s} = b - \beta si - bs + ais \tag{24}$$

$$\dot{e} = \beta si - (\alpha + b)e + aie \tag{25}$$

$$\dot{i} = \alpha e - (\gamma + a + b)i + ai^2 \tag{26}$$

$$\dot{r} = \gamma i - br + air \tag{27}$$

Calculating the Jacobian and evaluating at the disease-free equilibrium $(s, e, i) = (1, 0, 0)$ yields:

$$J(1, 0, 0) = \begin{bmatrix} -b & 0 & a - \beta \\ 0 & -(\alpha + b) & \beta \\ 0 & \alpha & -(\gamma + a + b) \end{bmatrix} \tag{28}$$

This gives us the following next generation operator:

$$FV^{-1} = \frac{1}{|V|} \begin{bmatrix} 0 & (a - \beta)\alpha b & (a - \beta)b(\alpha + b) \\ 0 & \beta\alpha b & \beta b(\alpha + b) \\ 0 & 0 & 0 \end{bmatrix} \tag{29}$$

where:

$$|V| = b(\alpha + b)(\gamma + a + b) \tag{30}$$

The spectral radius of the above yields the relationship between R_0 and β as [15]:

$$R_0 = \frac{\alpha\beta}{(b + \alpha)(b + a + \gamma)} \tag{31}$$

C. EFFECTS OF MEDIA: SOCIAL DISTANCING

Denote as m the proportion of people that have seen media broadcast about COVID-19 and/or possible recommendations concerning the stifling of the spread. σ is used to represent the proportion of people that are affected by the media and, thus, do what is necessary to keep themselves from encountering infected individuals. In this way, we see that $1 - m\sigma$ is the proportion of susceptible individuals that may potentially encounter infected individuals. If we apply this notion to the *SEIR* model introduced in the previous section, then we get the following updated model:

$$\dot{s} = b - \tilde{\beta}si - bs + ais \tag{32}$$

$$\dot{e} = \tilde{\beta}si - (\alpha + b)e + aie \tag{33}$$

$$\dot{i} = \alpha e - (\gamma + a + b)i + ai^2 \tag{34}$$

$$\dot{r} = \gamma i - br + air \tag{35}$$

where $\tilde{\beta} = \beta(1 - p)$ and $p = m\sigma$. Therefore, the amount of people that remove themselves from potential contraction

of the virus due to the media is directly related to the number of secondary infections, which has a large impact on altering the dynamics of the disease spread. When a fraction of the population, represented above as p , is protected from infection then the effective reproduction number becomes $R_e = (1 - p)R_0$, assuming a well-mixed population [16].

The effective reproductive number directly determines the number of secondary cases generated by an infected case once an epidemic is underway. Thus, we require that $R_e < 1$, although R_0 may not be below 1 [17]. For a population practicing social distancing, the proportion of susceptible individuals that are not practicing social distancing is represented by $1 - p$.

When measuring the effects of media coverage and social interactions on the spread of the disease a similar approach to Grassly *et al.* will be adopted in that an effective reproductive number will be calculated based on a media-informed population [9]. There is an optimal value of R_e that is needed to be reached to give an outbreak of the exact size that is needed to give enough population immunity. If the controls are too strong then an epidemic can occur once controls are lifted, and reintroduction of the disease occurs [18]. Social interactions and countermeasures will indeed play a key role on the spread of disease.

It has been shown that a small reduction in the basic reproduction number will have little effect on reducing the final proportion of people that are infected if the reproduction number was initially very high. On the other hand, if the reproduction number is not much greater than 1 then a small reduction in the basic reproduction number has a significant effect on reducing the proportion of individuals who will contract the virus [19]. Therefore, $R_e = 1$ represents a turning point in the long-term dynamics of the disease propagation.

IV. COMPUTER SIMULATIONS AND DISCUSSION

The aforementioned compartmental models represent a system of ordinary differential equations for which there are several numerical algorithms that provide an approximate solution. In this analysis, the linear multistep model known as the Adams-Bashforth method is chosen. This method has strong stability properties and is efficient to compute, provided that F_i is computed at each subsequent timestep t_i with associated state-space distribution Y_i .

In the following formulation, we use Y_i to represent current state values, which implies that $Y_i = (S, E, I, R)_i$. Provided the ODE system $\dot{Y} = F(t, Y)$, initial time t_0 , initial state-space distribution Y_0 , and timestep h , we first implement Euler's method represented by (36) followed by Adams-Bashforth two, three, and four-step explicit methods represented by (37), (38), and (39), respectively. For subsequent timesteps, the Adams-Bashforth five-step explicit method is used for the numerical approximations of Y_n as represented by (40) [20]:

$$Y_1 = Y_0 + hF_0 \tag{36}$$

$$Y_2 = Y_1 + h \left(\frac{3}{2}F_1 - \frac{1}{2}F_0 \right) \tag{37}$$

$$Y_3 = Y_2 + h \left(\frac{23}{12}F_2 - \frac{16}{12}F_1 - \frac{5}{12}F_0 \right) \quad (38)$$

$$Y_4 = Y_3 + h \left(\frac{55}{24}F_3 - \frac{59}{24}F_2 + \frac{37}{24}F_1 - \frac{9}{24}F_0 \right) \quad (39)$$

$$Y_n = Y_{n-1} + h \left(\frac{1901}{720}F_{n-1} - \frac{2774}{720}F_{n-2} + \frac{2616}{720}F_{n-3} \dots - \frac{1274}{720}F_{n-4} + \frac{251}{720}F_{n-5} \right), \quad n \geq 5 \quad (40)$$

where we used the shorthand $F_i = F(t_i, Y_i)$.

There is a vast amount of research being actively done on COVID-19 and studies have shown that the basic reproduction number, R_0 , is in the range of 1.5-3.5 with averages around 2.3 [21]. Incubation periods of 5-days have been used by the research team at John Hopkins University, which implies that the rate of transition from exposed to infected is $\alpha \approx 0.2$ [22], [23]. Recovery period estimates range from 5-days to 2-6 weeks in total, which implies that the recovery rate $\gamma \approx 0.024-0.2$ with typical values in the range $0.07 - 0.2$ [22]-[24].

Considering the current Canadian population, we set the initial population N_0 equal to an estimate of ~ 37.59 M. For birth and death rates, we will use estimates derived from global numbers [25]. Therefore, the value of b and d are:

$$b \approx 4.92985e - 5/\text{day} \quad (41)$$

$$d \approx 2.07234e - 5/\text{day} \quad (42)$$

For the incubation and infection periods, the global average values will be used for the COVID-19 outbreak:

$$\alpha = \gamma = 0.2 \quad (43)$$

To determine the parameters R_0 and a , a series of simulations using the SEIR model defined above were performed fitting the parameters that minimize the mean absolute error in the total caseload and total disease-related deaths. The mean absolute error in the total disease-related deaths were rescaled by the max total cases divided max total disease-related deaths so that the error in the total cases and disease-related deaths are of the same order.

The parameter estimation was performed prior to the introduction of social distancing measures to ensure that the values were not biased toward any social distancing measures [26]. For this study, the date of the introduction of social distancing was assumed to be on day 90 (April 14, 2020) following the first introduction of COVID-19 cases within Canada on January 15, 2020. Therefore, the parameter estimation considered up to and including April 13, 2020 and used the most recent 10 days in that period as validation for the parameters. Furthermore, the assumption was made that the number of reported cases is equivalent to 20% of the total number of cases based on early assumptions of mild/asymptomatic cases making up 80% of the total caseload [27]. Therefore, the predicted infected count which represents the total number of infected cases was reduced by a factor of 5 for comparison to the reported numbers.

To optimize the parameters, 861 simulations were performed where the disease-related-death rate ranged from 1% to 3% incrementing by 0.05% while R_0 ranged from 2 to 3 incrementing by 0.05. The optimal parameters identified were $R_0 = 2.65$ and $a = 0.0135$. This value of a is consistent with recent estimates of the infection fatality rate (IFR) [28], [29].

For dynamics to be created we merely need to initialize our system as $(s, e, i, r)_0 = (1, 0, 1/N_0, 0)$. It is of note that this represents only 1 infected individual being introduced into the population. Due to this fact, we later conclude why it is important that in a disease-free state we have very strict policies and testing procedures in place to ensure that reintroduction of infected individuals does not occur.

Although recent papers have provided evidence of pre-symptomatic transmission [30], [31], the aim of this paper is to provide a comparative study of the impacts of varying the seriousness of social distancing and the relationship that has on the spread of COVID-19 cases. Therefore, this comparative study uses the default SEIR model formulation with varying birth and death rates as well as disease-related deaths as introduced above. Furthermore, there are numerous approaches to studying social impacts over time such as Markov-based solutions for adaptive social networks [32] and time-varying social isolation parameters. However, for the purposes of comparison and given the nature of the recommendations provided to the Canadian population, the simplifying assumption of a constant social distancing impact was assumed in this study.

A. SIMULATION 1: BASELINE

Using the above default parameter values, incorporating no media or other preventative measures, we get a worst-case baseline scenario. For this simulation, unconstrained exponential growth occurs due to the interaction term βsi . When the susceptible population is infected and subsequently recovers from the virus, they are assumed to have immunity. As well, through natural births the susceptible population continues to grow over time. However, through the exponential growth of the infected population the susceptible population is more quickly depleted than replenished through natural births and a critical point is reached for which a decline in the incidence of the virus occurs. Although worst case scenario, this does result in a ‘disease-free’ state occurring quite rapidly as the virus quickly spreads through most of the population. Figure 4 shows the dynamics of this simulation.

From the simulation, it is found that, under no preventative measures, the virus would infect approximately 87.35% of the population. This number represents the percentage of the susceptible group and, since we assume that no preventative measures is taken, we assume the susceptible group is indeed the entire population. Using the entire population of Canada as the sample group for this simulation, we see that this represents approximately 34.46 M people being infected with the virus over the year. The entire disease-related death count

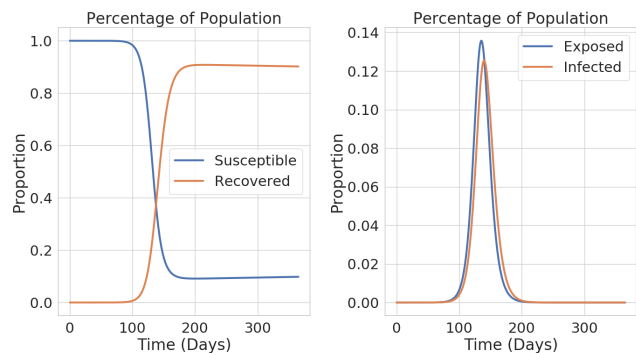


FIGURE 4. Results of a baseline simulation that shows the proportion of individuals that are in the susceptible and recovered states (left) as well as the exposed and infected states (right) over time.

would be approximately 458.9 k and the disease would exit the population on day 308. Since the first case occurred in Canada on January 15, 2020 this would imply a disease-free state on November 18, 2020.

B. SIMULATION 2: FLATTENING OF THE CURVE

Social distancing plays a critical role in the flattening of the curve. This first set of results focusses on cases for which p is not large enough to reduce the effective reproductive number below 1 which would result in halting the spread, explored in the next section. However, the flattening of the curve introduced in these simulations still has significant impacts on the disease spread. Depending on the proportion of individuals removed from the susceptible population through these efforts, it has the impact of both reducing the peak and increasing the time to the peak in infected cases. Through flattening of the peak, it reduces the likelihood of overwhelming Canada’s healthcare system and extending the timeline of the spread provides more time for either the development of a vaccine or more rigorous test regimes. Vaccines again have the direct impact of reducing the susceptible population, however more rigorous test regimes also have the direct impact of determining and isolating infected individuals more rapidly. This can allow for more precise isolation tactics.

For these simulations, we assume that at the 90-day point of the disease-progression that social distancing efforts have begun. Although a simplified assumption, it offers the ability to give easy comparison of various social distancing impacts. For this grouping of results, we consider cases for when the social distancing efforts have reduced the susceptible population by 15% to 55% in 10% increments. This is equivalent to values of p ranging from 0.15 to 0.55.

Table 1 offers a comparison of the various scenarios which result in the flattening of the curve. In this table, we use TI to indicate total infected, TDRD for total disease-related deaths, DFD for disease-free days or the number of days until a disease-free state occurs, and DFDT for the disease-free date or approximate date at which disease-free state occurs. In addition, in Fig. 5, we see the impacts on the proportion of the population that are within the infected state

TABLE 1. Comparison of the various flattening scenarios.

p	TI	TDRD	DFD	DFDT
0.00	34,460.2 k (87.35%)	458.92 k	308	Nov. 18, 2020
0.15	32,367.8 k (82.04%)	431.06 k	348	Dec. 28, 2020
0.25	30,122.9 k (76.35%)	401.16 k	391	Feb. 09, 2021
0.35	26,695.4 k (67.66%)	355.51 k	462	Apr. 21, 2021
0.45	21,233.2 k (53.81%)	282.77 k	603	Sep. 09, 2021
0.55	12,075.4 k (30.60%)	160.81 k	1,025	Nov. 05, 2022

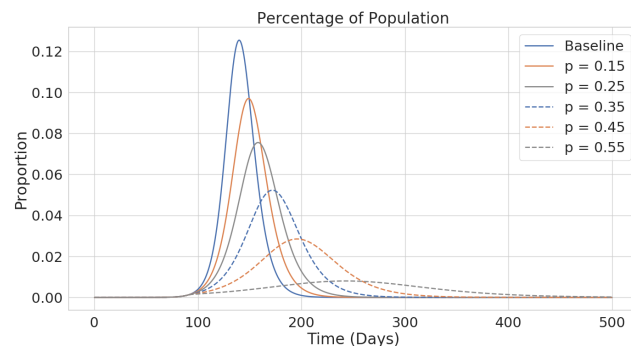


FIGURE 5. Proportion of the population considered infected, demonstrating the ‘flattening of the curve’ behavior. Fewer people are infected but it takes a significantly longer time for the virus to work through the entire population.

over time. With increasing values of p the peak flattens more dramatically as well as shifts later into the future.

Contrasting the cases for which $p = 0.25$ and $p = 0.55$ to the baseline scenario above, we see modest and more extreme reductions in the total infected and disease-related deaths, respectively. In the former case, the maximum proportion of the population that is infected at the peak of the pandemic is approximately 7.5% in contrast to the base case for which the maximum proportion is approximately 12.5%. In the latter case, the maximum proportion of the population infected at a given point reduces even further to 0.8%. The evolution of the exposed and infected states is shown in Fig. 6 for these two scenarios.

C. SIMULATION 3: HALTING THE SPREAD

If we continue to increase the impact of social distancing by further increasing the value of p , then we will begin to enter the region where the effective reproductive rate falls below 1. In this case the disease spread will begin to halt. As the effective reproductive number becomes smaller the halting of the disease spread occurs more rapidly. This is essentially due to the balance between the incubation period, infection period, and further exposure of individuals to the virus which occurs at a reduced rate.

However, once the population has reached a disease-free point, it is extremely important to note that if a single new case is reintroduced into the population, then a new epidemic will occur. Therefore, it is paramount that ongoing rigorous testing is performed at the border to prevent reintroduction of an infected individual until globally COVID-19 has been eradicated.

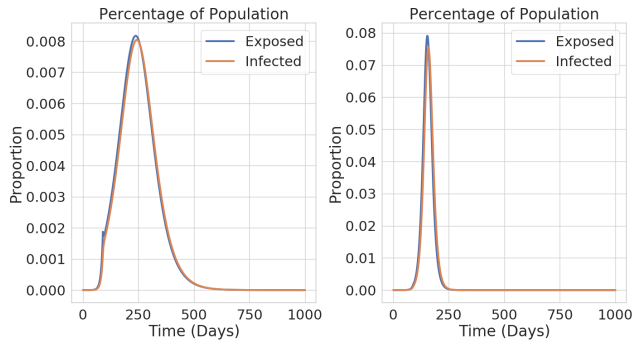


FIGURE 6. Proportion of the population exposed and infected over time for the cases when social distancing has removed $p = 0.25$ (left) and $p = 0.55$ (right) from the susceptible population 90 days after the first reported case within Canada.

TABLE 2. Comparison of the various halting scenarios.

p	TI	TDRD	DFD	DFDT
0.00	34,460.2 k (87.35%)	458.92 k	308	Nov. 18, 2020
0.65	1,322.9 k (3.35%)	17.62 k	1,200	Apr. 29, 2023
0.70	603.1 k (1.53%)	8.03 k	592	Aug. 29, 2021
0.75	401.4 k (1.02%)	5.35 k	394	Feb. 12, 2021
0.80	309.6 k (0.78%)	4.12 k	301	Nov. 11, 2020
0.85	257.4 k (0.65%)	3.43 k	246	Sep. 17, 2020
0.90	223.8 k (0.57%)	2.98 k	210	Aug. 12, 2020
0.95	200.3 k (0.51%)	2.67 k	184	Jul. 17, 2020
1.00	183.0 k (0.46%)	2.44 k	162	Jun. 25, 2020

To simulate the various halting cases, we consider where $(1 - p)R_e < 1$ which occurs for $p \geq 62.3\%$. Therefore, we consider the cases for $p = 0.65$ to $p = 1$ in increments of 0.05. The key metrics for these simulations are summarized in Table 2 while the time-series of the proportion of infected individuals is summarized in Fig. 7.

It is observed that the impacts are significantly more dramatic in comparison to the flattening cases from the past subsection. In particular, even in the most conservative halting case for which $p = 0.65$, we observe that the peak dramatically reduces from approximately 12.5% of the population being infected at the peak of the pandemic to only 0.14%. Furthermore, the number of disease-related deaths is reduced by a factor of 26 even for this conservative case. However, because the disease progression continues while the active caseload slowly diminishes, a disease-free state does not occur until day 1,200 or April 29, 2023. On the other hand, if we consider a more strict enforcement where $p = 0.8$ the total disease-related deaths could have been reduced to a total of approximately 4.12 k and the disease-free date would occur roughly around the same time as the base case on November 11, 2020.

D. COMPARISON TO ACTUAL CASE NUMBERS

At the time of writing this article, the total number of reported cases had reached approximately 101 k and the total of disease-related deaths had reached approximately 8.4 k in Canada. To compare the simulated results with the actual cases, we consider the range of halting strategies from

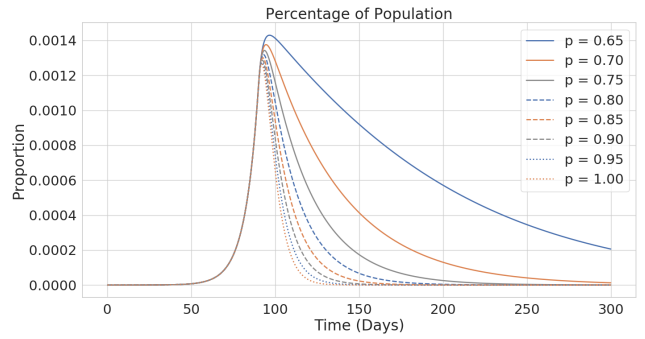


FIGURE 7. Proportion of the population considered infected, demonstrating the ‘halting of the virus’ behavior. The result of which is a significant reduction in the peak of the infected numbers.

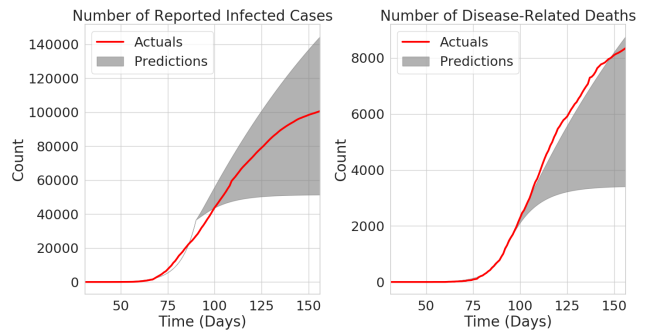


FIGURE 8. Comparison of the predicted total number of cases and total-disease related deaths for the range of halting strategies from $p = 0.65$ to $p = 0.85$ overlain with the actuals up until June 20, 2020.

$p = 0.65$ to $p = 0.85$. The comparison to the actual values are shown in Fig. 8. We see that the total number of cases aligns closely to an intermediate p value between 0.65 and 0.85 (with subsequent analysis showing very close alignment to $p = 0.7$) while the total disease-related deaths for this same case would be slightly understated from the actual numbers. This is possibly due to a slightly higher disease-related death rate than what was observed from the initial numbers and/or a higher number of non-reported COVID-19 cases. Furthermore, it may be due to the drastic effects of hot spots forming in long-term care homes which was not included in the modeling.

E. SUBSEQUENT REDUCTION IN SOCIAL DISTANCING

Although the simplifying assumption of constant social distancing from day 90 onward used in this study is not representative of the dynamic situation of reality, we observed in the previous subsection that the results obtained do have alignment with realistic values. Furthermore, the comparison of lenient versus strict social distancing strategies showcase the importance social distancing has on the spread and the resulting disease-related deaths.

However, as Canada enters the next phase of the pandemic where businesses begin to reopen and society returns to some semblance of normalcy, it bodes the question of how vigilant the Canadian population should remain. Before considering simulations to showcase the potential spread,

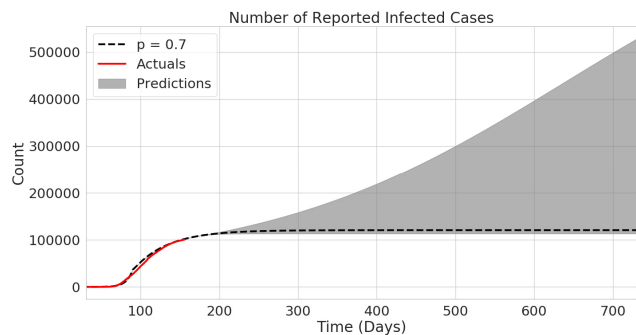


FIGURE 9. Comparison of the predicted total caseload for the $p = 0.7$ case at day 90 followed by subsequent changes of p at day 180 from $p = 0.6$ (relaxed social distancing) to $p = 0.8$ (more strict social distancing).

epidemiological theory tells us that if the effective reproductive rate exceeds 1 then caseloads will again increase. However, it should be noted that this spread is both a function of R_e as well as the number of susceptible individuals. If the number of susceptible individuals is sufficiently small, then the caseload will continue to decline (i.e., herd immunity).

Using the approximate best fit scenario of $p = 0.7$ introduced at day 90, we integrate forward the SEIR ODE equations to day 180 where we subsequently modify the social distancing parameter. At day 180, we consider the range of cases for $p = 0.6$ to $p = 0.8$. The relaxed, $p = 0.6$ case represents where the effective reproductive number exceeds 1.06 and we see that without further policies or procedures implemented the case numbers continue to grow to the end of the 2-year period considered. On the other hand, if social distancing measures represented by $p = 0.7$ is maintained or further increased to $p = 0.8$, then the case numbers only marginally increase from those observed at the day of writing.

V. LIMITATIONS OF THE STUDY

This study considers a simplified approach to analyzing the impacts of social distancing by introducing point-in-time coefficients that influences the proportions of individuals in the susceptible population. The authors recognize that social distancing measures are stochastic in nature, however this study aims at the implications that different degrees of social distancing could have on the caseload evolution. Also, using the entire Canadian population as potential susceptible individuals is another simplifying assumption and subsequent studies will be aimed at considering smaller segments of the population.

Several of the model parameters used in the simulations are based on global studies. These may be pessimistic or optimistic in contrast to the actual values observed in the Canadian population. In order to ensure the numbers are most representative for Canada, further simulations can be performed in order to optimize other parameters based on the current observations in Canada. However, extending the search space using a naïve grid search approach quickly makes the computational requirements infeasible.

Therefore, other types of parameter estimation approaches such as Tree Parzen Estimators will need to be explored for these subsequent studies. Furthermore, the non-reporting factor of 5 was used based on the mild and asymptomatic cases and as more accurate evaluation of the total caseload and total deaths (rather than reported numbers) becomes available, it will be important to update the non-reporting factor for caseloads as well as introduce the same for total deaths.

Given the recency of the COVID-19 outbreak, it was assumed that maternally derived immunity would not impact the current dynamics of the simulations. However, with ongoing progression of the COVID-19 pandemic, it will become more and more important to adapt this SEIR model into more robust alternatives such as the MSEIR model.

Lastly, although comparisons with other countries was not performed in this study, similar approaches can be leveraged and contrasted with those geographic regions and could make for an interesting subsequent comparative study. However, this current paper aimed to fill a gap in these types of studies within the Canadian population.

VI. DISCUSSION

As simulated, social distancing can have a dramatic impact on the containment of COVID-19. As social distancing ends or driving the effective reproductive number below 1, significant impacts are observed which are consistent with the findings of Koopman *et al.* [19]. If we had overly strong compliance with social distancing and 80% of the population removed themselves from the susceptible population by taking the precautionary steps to ensure non-exposure, then the estimated result would have yielded 309.6 k total infected cases (and an expected 61.92 k reported), 4.12 k disease-related deaths, and a disease-free date of approximately November 11, 2020 which is near to the catastrophic baseline of November 18, 2020. Through comparison with the current total caseload and subsequent simulations showing progression under different social distancing regimes, we see that if policies and procedures remain in effect that remove 70% of individuals exposure to COVID-19, then the number of reported cases is not likely to exceed approximately 120 k. Rigorous testing, targeted social distancing, and isolation could help to increase the mobility of Canadian residents while minimizing likelihood of exposure to COVID-19.

Furthermore, it should be noted that no matter the age group, you can contract the virus and there is a lot of evidence supporting the likelihood of individuals showing mild to no symptoms. This is a huge danger of COVID-19 as individuals who have little to no symptoms may refrain from social distancing. In particular, the younger population is not immune and can be carriers of the virus.

Blanket social distancing does not need to be the only policy but, in lieu of rigorous and widespread testing, it may be the best policy. If we establish a more widespread test regime, then we could have more isolated social distancing measures that target those that test positive. Without such

testing regimes however, travel-based isolation strategies offer an example strategic alternative. That is, enforcing self-isolation for those individuals that have travelled due to the higher probability of them having been exposed to the virus.

VII. CONCLUSIONS

In this paper, baseline compartmental models used for modelling infectious diseases were utilized and coefficients to model social distancing were proposed. The impacts of social distancing were studied and explored through numerical simulations. Robust and accurate numerical approximation techniques were used to simulate the pessimistic base case for which no preventative measures are taken and for various social distancing regimes. It was discovered that social distancing efforts can significantly reduce the spread of COVID-19 by two orders of magnitude based on the simulations completed.

The results of social distancing were consolidated into two groups – those that flatten the curve and those that completely halt the spread. Mathematical formulations show that the turning point between these two groups is when the effective reproductive rate is equal to 1. However, it is important to note that the proposed models do not take into consideration the effects of clusters or viral hot spots forming such as in retirement homes, long-term care homes, or agricultural processing plants. These events can cause increased cases of COVID-19 which would increase the spread of the virus.

Subsequent simulations comparing results to observed values showcase that even simple formulations can have some bearing on reality, as well as provide interesting findings for which relative comparisons can be made. Furthermore, applying a similar range of social distancing strategies to simulate impacts upon reopening the economy sheds light on the need to remain vigilant until COVID-19 is completely removed from the Canadian population and/or a vaccine is developed.

If we adopt the technology we are so fortunate to have today to effectively work remotely, remain with immediate family members, limit exposure to others, practice social distancing when in public, and self-isolate as required, then the effects of COVID-19 on the population (societal and economical) can be minimized.

REFERENCES

- [1] Z. Wu and J. M. McGoogan, "Characteristics of and important lessons from the coronavirus disease 2019 (COVID-19) outbreak in China: Summary of a report of 72 314 cases from the Chinese center for disease control and Prevention," *J. Amer. Med. Assoc.*, vol. 323, no. 13, pp. 1239–1242, 2020.
- [2] R. M. Anderson, H. Heesterbeek, D. Klinkenberg, and T. D. Hollingsworth, "How will country-based mitigation measures influence the course of the COVID-19 epidemic?" *Lancet*, vol. 395, no. 10228, pp. 931–934, Mar. 2020.
- [3] G. Krr and F. Casella. (Mar. 25, 2020). *Non-Pharmaceutical Interventions (NPIs) to Reduce COVID-19 Mortality*. [Online]. Available: <https://ssrn.com/abstract=3560688>
- [4] K. Sun, J. Chen, and C. Viboud, "Early epidemiological analysis of the coronavirus disease 2019 outbreak based on crowdsourced data: A population-level observational study," *Lancet Digit. Health*, vol. 2, no. 4, pp. e201–e208, Apr. 2020.
- [5] B. J. Cowling, S. T. Ali, T. W. Ng, T. K. Tsang, J. C. Li, M. W. Fong, Q. Liao, M. Y. Kwan, S. L. Lee, S. S. Chiu, and J. T. Wu, "Impact assessment of non-pharmaceutical interventions against COVID-19 and influenza in Hong Kong: An observational study," in *Proc. MedRxiv*, 2020, p. 29.
- [6] L. Li, Q. Zhang, X. Wang, J. Zhang, T. Wang, T.-L. Gao, W. Duan, K. K.-F. Tsoi, and F.-Y. Wang, "Characterizing the propagation of situational information in social media during COVID-19 epidemic: A case study on Weibo," *IEEE Trans. Comput. Social Syst.*, vol. 7, no. 2, pp. 556–562, Apr. 2020.
- [7] L. Zhong, L. Mu, J. Li, J. Wang, Z. Yin, and D. Liu, "Early prediction of the 2019 novel coronavirus outbreak in the mainland China based on simple mathematical model," *IEEE Access*, vol. 8, pp. 51761–51769, 2020.
- [8] M. Y. Li, J. R. Graef, L. Wang, and J. Karsai, "Global dynamics of a SEIR model with varying total population size," *Math. Biosci.*, vol. 160, no. 2, pp. 191–213, Aug. 1999.
- [9] N. C. Grassly and C. Fraser, "Seasonal infectious disease epidemiology," *Proc. Roy. Soc. B, Biol. Sci.*, vol. 273, no. 1600, pp. 2541–2550, 2006.
- [10] J. D. Mathews, C. T. McCaw, J. McVernon, E. S. McBryde, and J. M. McCaw, "A biological model for influenza transmission: Pandemic planning implications of asymptomatic infection and immunity," *PLoS ONE*, vol. 2, no. 11, p. e1220, Nov. 2007.
- [11] J. M. Heffernan, R. J. Smith, and L. M. Wahl, "Perspectives on the basic reproductive ratio," *J. Roy. Soc. Interface*, vol. 2, no. 4, pp. 281–293, Sep. 2005.
- [12] P. van den Driessche and J. Watmough, "Reproduction numbers and sub-threshold endemic equilibria for compartmental models of disease transmission," *Math. Biosci.*, vol. 180, nos. 1–2, pp. 29–48, Nov. 2002.
- [13] C. Viboud, T. Tam, D. Fleming, A. Handel, M. A. Miller, and L. Simonsen, "Transmissibility and mortality impact of epidemic and pandemic influenza, with emphasis on the unusually deadly 1951 epidemic," *Vaccine*, vol. 24, nos. 44–46, pp. 6701–6707, Nov. 2006.
- [14] C. Sun and Y.-H. Hsieh, "Global analysis of an SEIR model with varying population size and vaccination," *Appl. Math. Model.*, vol. 34, no. 10, pp. 2685–2697, Oct. 2010.
- [15] J. Li and N. Cui, "Dynamic analysis of an SEIR model with distinct incidence for exposed and infectives," *Sci. World J.*, vol. 2013, pp. 1–5, May 2013.
- [16] G. Chowell, H. Nishiura, and L. M. A. Bettencourt, "Comparative estimation of the reproduction number for pandemic influenza from daily case notification data," *J. Roy. Soc. Interface*, vol. 4, no. 12, pp. 155–166, Feb. 2007.
- [17] M. Lipsitch, T. Cohen, B. Cooper, J. M. Robins, S. Ma, L. James, G. Gopalakrishna, S. K. Chew, C. C. Tan, M. H. Samore, and D. Fisman, "Transmission dynamics and control of severe acute respiratory syndrome," *Science*, vol. 300, no. 5627, pp. 1966–1970, Jun. 2003.
- [18] M. C. J. Bootsma and N. M. Ferguson, "The effect of public health measures on the 1918 influenza pandemic in U.S. Cities," *Proc. Nat. Acad. Sci. USA*, vol. 104, no. 18, pp. 7588–7593, May 2007.
- [19] J. S. Koopman, D. R. Prevots, M. A. V. Mann, H. G. Dantes, M. L. Z. Aquino, I. M. Longini, and J. S. Amor, "Determinants and predictors of dengue infection in Mexico," *Amer. J. Epidemiol.*, vol. 133, no. 11, pp. 1168–1178, Jun. 1991.
- [20] R. L. Burden and J. D. Faires, "Multistep methods," in *Numerical Analysis*, 8th ed. Boston, MA, USA: Cengage Learning, 2005.
- [21] N. Imai, A. Cori, I. Dorigatti, M. Baguein, C. A. Donnelly, S. Riley, and N. M. Ferguson, "Transmissibility of 2019-nCoV," Imperial College London, London, U.K., Tech. Rep. 3, Jan. 2020, doi: [10.25561/77148](https://doi.org/10.25561/77148).
- [22] L. Gardner, "Update January 31: Modeling the spreading risk of 2019-nCoV," Johns Hopkins Univ. Center Syst. Sci. Eng., Baltimore, MD, USA, Tech. Rep., Jan. 2020.
- [23] Q. Li et al., "Early transmission dynamics in Wuhan, China, of novel coronavirus-infected pneumonia," *New England J. Med.*, vol. 382, pp. 1199–1207, Mar. 2020.
- [24] *Report of the WHO-China Joint Mission on Coronavirus Disease 2019 (COVID-19)*, World Health Org., Geneva, Switzerland, 2020.
- [25] Worldometer. *Worldometer-Real Time World Statistics*. Accessed: Jun. 23, 2020. [Online]. Available: <https://www.worldometers.info>
- [26] B. C. K. Choi, "A simple approximate mathematical model to predict the number of severe acute respiratory syndrome cases and deaths," *J. Epidemiol. Community Health*, vol. 57, no. 10, pp. 831–835, Oct. 2003.
- [27] *Coronavirus Disease 2019 (COVID-19): Situation Report, 46*, World Health Org., Geneva, Switzerland, 2020.

[28] A. Basu, "Estimating the infection fatality rate among symptomatic COVID-19 cases in the United States: Study estimates the COVID-19 infection fatality rate at the U.S. County level," *Health Affairs*, vol. 39, no. 7, pp. 1310–1377, 2020.

[29] T. S. Coleman, "Estimating lower bounds for COVID-19 mortality from Northern Italian towns," in *Proc. MedRxiv*, 2020, pp. 1–13.

[30] Y. Bai, L. Yao, T. Wei, F. Tian, D. Y. Jin, L. Chen, and M. Wang, "Presumed asymptomatic carrier transmission of COVID-19," *J. Amer. Med. Assoc.*, vol. 323, no. 14, pp. 1406–1407, 2020.

[31] L. Tindale, M. Coombe, J. E. Stockdale, E. Garlock, W. Y. V. Lau, M. Saraswat, Y. H. B. Lee, L. Zhang, D. Chen, J. Wallinga, and C. Colijn, "Transmission interval estimates suggest pre-symptomatic spread of COVID-19," in *Proc. MedRxiv*, 2020, p. 30.

[32] C. Liu, N. Zhou, X.-X. Zhan, G.-Q. Sun, and Z.-K. Zhang, "Markov-based solution for information diffusion on adaptive social networks," *Appl. Math. Comput.*, vol. 380, Sep. 2020, Art. no. 125286.



JOHN YAWNEY received the Ph.D. degree in applied mathematics from the University of Waterloo. He is currently a Chief Analytics Officer with Adastra, Markham, ON, USA, where he leads the data science practice. He is currently an Adjunct Professor with the University of Guelph. He has extensive experience performing numerical and statistical analyses. His past research experiences include computational fluid dynamics simulations leveraging HPC clusters, geospatial analysis of waterbodies incorporating underlying stream networks, and exploration into epidemiological model development. His practical development exposures include several languages (R, Python, C, C++, SQL, Spark) and with numerous tools within the Hadoop ecosystem. Throughout his professional career, the models and analyses he has been responsible for range from simple statistical testing, univariate and multivariate regression, to complex LSTM and deep learning models. The models he has developed include structured data, semi-structured text data, and unstructured sources including audio and video data sources. Since starting his leadership role as Adastra's data science practice lead, he has grown the team five-fold with a successful, healthy project pipeline.



STEPHEN ANDREW GADSDEN (Senior Member, IEEE) received the bachelor's degree in mechanical engineering and management (business) and the Ph.D. degree in mechanical engineering in the area of estimation theory from McMaster University. He worked as a Postdoctoral Researcher with the Centre for Mechatronics and Hybrid Technology, Hamilton, ON, Canada. He also worked as a Project Manager in the pharmaceutical industry (Apotex Inc.) for three years. He is currently an Associate Professor of in mechanical engineering with the University of Guelph. Before joining Guelph, he was an Assistant Professor with the Department of Mechanical Engineering, The University of Maryland, Baltimore County, USA. He has a number of colleagues in NASA, the U.S. Army Research Laboratory (ARL), the U.S. Department of Agriculture (USDA), the National Institute of Standards and Technology (NIST), and the Maryland Department of the Environment (MDE). He is an elected Fellow of ASME and a Professional Engineer of Ontario. He received the 2019/2020 University Research Excellence Award for the College of Engineering and Physical Sciences based on his research activities at the University of Guelph. In addition, he received the 2019 SPIE Rising Researcher Award winner based on his work in intelligent estimation theory, and the 2018 Ontario Early Researcher (ERA) Award winner based on his work in intelligent condition monitoring strategies. He also won the 2019 University of Guelph Faculty Association (UGFA) Distinguished Professor Award for Excellence in Teaching in the College of Engineering and Physical Sciences at the University of Guelph.

...